Biosensors and Bioelectronics 146 (2019) 111743

Contents lists available at ScienceDirect

Biosensors and Bioelectronics

journal homepage: http://www.elsevier.com/locate/bios

Electroactive metal–organic framework composites: Design and biosensing application

Xianjiu Liao [a,b], Haomin Fu [b], Tingting Yan [b], Jianping Lei [b,*]

[a] School of Pharmacy, Youjiang Medical University for Nationalities, Baise, Guangxi, 533000, China
[b] State Key Laboratory of Analytical Chemistry for Life Science, School of Chemistry and Chemical Engineering, Nanjing University, Nanjing, 210023, China

ARTICLE INFO

Keywords:
Metal-organic frameworks
Biosensors
Electrochemistry
Modification
Signal transduction
Nanoparticles

ABSTRACT

Metal-organic frameworks (MOFs) as molecular crystalline materials have been extensively applied in various fields such as catalysis, separation, and biomedical engineering. However, the applications of MOFs materials are limited in electrochemical biosensing due to the poor conductivity, less selectivity, and lack of modification sites. By incorporating the functionalized nanoparticles into MOF structures, MOF-based composites are endowed with high electronic conductivity and strong catalytic activity, which process the advantages over single-component MOFs. With a particular focus on the electrochemical applications of MOF composites, this review summarizes the comprehensive guidelines on design of electroactive MOF composites: dopant modification of electroactive ligands, in situ synthesis of nanoparticle@MOF composites and post-modification of MOF structure. The illustrative examples of electroactive MOF composites in the last five years are highlighted in electrochemical, electrochemiluminescent, and photoelectrochemical biosensing. The prospects and challenges for future work are also included. Understanding the structure-function relationship of electroactive MOF composites benefits the design of next-generation electrochemical biosensors.

1. Introduction

Metal-organic frameworks (MOFs) are the emerging molecular crystalline materials, which have attracted great attention in catalysis, separation, and biomedical applications due to the unique structural features and the excellent optoelectronic properties (Cho et al., 2019; Diercks et al., 2018; Dolgopolova et al., 2018; Lu et al., 2018a, 2018b; Zhao et al., 2018). MOFs have also been regarded as a promising candidate of electrochemical (EC) sensing material because of the high mass transfer capacities in controlled porous structure (Xue et al., 2019). For example, due to the high porosity and large surface area, zeolitic imidazolate frameworks (ZIFs) as the supporting matrix are believed to concentrate more dehydrogenase for in vivo electrochemical measurement of neurochemicals (Ma et al., 2013). However, the poor conductivity and unstable nature in aqueous solution of MOFs materials limit their further applications in electrochemical biosensors. An effective approach to overcome this obstacle is coupling MOFs and conductive substances into a single nanostructure (Liu et al., 2019a). The high conductivity materials (carbon materials, metal nanoparticles, etc.) encapsulated into MOF structures are helpful to enhance the electrochemical activities (Xu et al., 2018b). There are three different strategies to modify MOFs composite: dopant modification, in situ entrapping functional molecules or nanoparticles (NPs) within the framework, and post-modification methods (Hassanzadeh et al., 2018), which provide the great potentials for electrochemical application.

MOF-based composite materials bearing high electronic conductivity and strong catalysis capacity usually combine the merits of both MOFs and guest materials, which can overcome the defects of single-component MOFs (Li et al., 2018a). Yang et al. used the gold nanoparticles (AuNPs) and MOF composites as signal probes to establish an electron transfer-mediated ultrasensitive electrochemical immunoassay for detection of the C-reactive protein (Liu et al., 2016). Furthermore, the catalytic sites in MOFs are readily accessible to enhance electrocatalytic efficiency. For example, a cobalt−porphyrin MOF was functionalized as catalyst for selectively electrocatalytic reduction of carbon dioxide to carbon monoxide in aqueous electrolytes (Kornienko et al., 2015). The platinum nanoparticles homogeneously immobilized on MOFs possess high stability and catalase-like activity to facilitate the transformation of H_2O_2 to O_2 (Zhang et al., 2018b).

Also, MOFs have received growing interest in electrochemiluminescence (ECL) assays, in which electrochemically triggered optical radiation process is produced by the energy relaxation of excited

* Corresponding author.
E-mail address: jpl@nju.edu.cn (J. Lei).

https://doi.org/10.1016/j.bios.2019.111743
Received 26 July 2019; Received in revised form 8 September 2019; Accepted 28 September 2019
Available online 30 September 2019

species, because they can provide a high specific surface for loading a large quantity of ECL luminophores. Different from the conventional metal complexes, luminol, and quantum dots as ECL luminophores, MOFs made metal porphyrin as organic ligand, have attracted much attention to act as ECL luminophores due to the high efficiency and excellent stabilities. For example, an ECL-active MOF was designed by using ruthenium complexes as ligands with the aid of grapheme oxide (GO) to enhance electron transfer (Xu et al., 2015). On the other hand, under irradiation, photoelectrochemical (PEC) technique has been developed based on the generation of photoelectric signal from electron transfer among analyte, photoactive MOFs, and electrode. Overall, the variation of response signal entirely depends on the MOF optoelectronic structure and the excitation signal.

Therefore, the potential advantages of integrating MOFs and electrochemical process are significant, but MOF-based electrochemical systems are less advanced (Qiu et al., 2019). First of all, this review analyses the essential relationship between the structure of MOF composite and electron transfer, and exploits the functionalization approach to enhance the electrochemical activities for the design patterns of electroactive MOF. Secondly, the comprehensive signaling transduction strategies of MOF composites are highlighted in electrochemical, electrochemiluminescent, and photoelectrochemical biosensing (Fig. 1). The summary of MOF-based biosensors with different signaling principles is listed in Table 1. Finally, the perspectives and challenges for future work have been proposed, providing the promising potentials in MOF-based electrochemical devices.

2. Assembly of MOF composites

The use of the single-component MOFs as electrode materials for electrochemical sensor construction usually results in narrow linear range, low sensitivity, and insufficient stability due to their low electronic conductivity, and/or poor electrocatalytic ability. By virtue of the advantages of MOFs, like tunable pores, diverse functional sites, and large surface area, a variety of functional sites/groups can be introduced into metal ions/clusters, organic linkers, or pore spaces through predesigning or post-synthetic approaches (Li et al., 2016; Ling et al., 2018; Pan et al., 2018). Moreover, the introduction of biomolecules including enzymes, nucleic acids, and peptides on the surface or in the cavity of MOFs enables the highly versatile sensing platform with enhanced sensitivity and specificity (Kempahanumakkagari et al., 2018).

2.1. Modification with electroactive ligands

By taking advantage of their synthetic tunability and structural regularity, MOFs can hierarchically integrate catalytic components into a single porous material through the use of pendant functional groups from the linker moiety of MOF (Mao et al., 2018; Wang et al., 2018a). Particularly, MOFs constructed with porphyrin subunits are interesting since porphyrins have the strong catalytic ability for signal readout. These porphyrin-based materials such as MOF-525 have high specific surface areas, and the electrochemical activity of the porphyrin subunit that can be tuned for different electrochemical sensing applications. A nanoscaled porphyrinic MOF was designed with iron porphyrin as linker and zirconium ion as node, and demonstrated excellent electrocatalytic activity toward O_2 reduction (Ling et al., 2016b). Interestingly, the organic building units, in the form of cobalt-metalated tetrakis(4-carboxyphenyl)porphyrin (TCPP), are assembled into a three-dimensional (3D) MOF (Fig. 2A), which was selected to construct the MOF-based electrochemical CO_2 reduction system with a per-site turnover number of 1400 (Kornienko et al., 2015). Furthermore, PtPd NPs were decorated on the electroactive Co-MOFs, which were not only used as nanocarriers but also acted as signal labels, and promoted the conversion of Co^{2+} to Co^{3+} on the frame, leading to excellently electrochemical signal amplification (Yang et al., 2017b).

Ruthenium (Ru) complexes could be properly treated to combine with the functional MOF (Ru-MOF) through metal ion chelation (Kozachuk et al., 2014). Ru-MOF nanoflowers were prepared by a one-step solvothermal method at low temperature (Fig. 2B). Since Ru-MOF was more accessible for efficient electron transfer based on its well-ordered structure, good stability and high catalytic efficiency, an enhanced ECL system was constructed with the aid of quantum dots (QDs) as coreactants (Zhu et al., 2017).

Interestingly, the developed metal-ligand-fragment co-assembly strategy could effectively work to introduce a wide variety of functional groups into MOFs, in which the primitive ligand and the ligand fragment were co-assembled to generate a series of the isostructural MOFs. For example, a mixed-ligand MOF was afforded via a solvothermal reaction between H_2DBP-Pt, H_2QPDC-NH_2, and $HfCl_4$ in N,N-dimethylformamide at 80 °C and then applied in intracellular oxygen biosensing (Xu et al., 2016). It worth mentioning that boronic acid functionalized ligand was co-assembled into Material of Institute Lavoisier (MIL)-100(Cr) as an efficient immobilization matrix of horseradish peroxidase for electrochemical detection of H_2O_2 (Dai et al., 2017).

In addition, a single-atom catalyst, Cu/UiO (University of Oslo)-66 was prepared by a covalent attachment of Cu atoms to the defect sites at the zirconium oxide clusters of the MOF UiO-66 (Fig. 2C). Density functional theory (DFT) calculations in combination with experimental data show that Cu binds to the MOF by –OH/−OH_2 ligands capping the defect sites at the Zr oxide clusters. This catalyst is highly active and stable under realistic reaction conditions with an excellent selectivity of about 100% for CO oxidation (Abdel-Mageed et al., 2019). Mirkin's group reported a coordination chemistry-based strategy for the surface functionalization of the external metal nodes of MOFs with terminal phosphate-modified oligonucleotides (Wang et al., 2017a). A series of uniform nanometer-sized MOFs, including monometal and bimetal (CoZn-ZIF), can be readily synthesized onto hierarchically structured flowerlike MgAl-layered double hydroxide supports with high dispersion and precision, which are beneficial to materials utilization and mass transport (Li and Zeng, 2016).

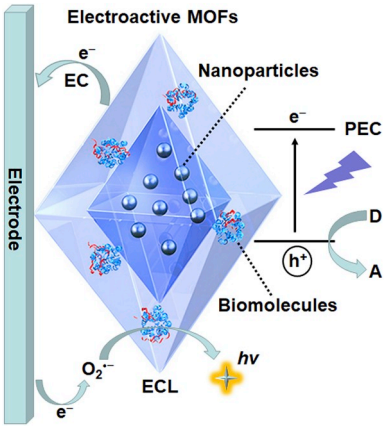

Fig. 1. Schematic illustration of the functionalization of electroactive MOF composite and its applications in electrochemical (EC), electrochemiluminescent (ECL), and photoelectrochemical (PEC) biosensing.

2.2. In situ synthesis of NP@MOF composites

To enhance their conductivity and catalysis ability, an applicable strategy was to construct MOF-based heterostructure with a customized selection of functional nanoparticle such as metal NPs, metal oxide (Koo et al., 2016; Lu et al., 2012), and carbon-based nanomaterials (Micheroni et al., 2018). According to the dimensionality of the MOF complex, NP@MOF composites were classified into four types such as zero-dimensional, one-dimensional, two-dimensional (2D), and 3D

Table 1
Summary of various signaling strategies for the electroactive MOF composites.

MOF composite for signaling strategy	Analyte	Linear range	Detection limit	Reference
EC strategies				
Fe-based-MOFs deposited with Au NPs as active sites to capture primary antibodies and accelerate the electron transfer	Galectin-3	100 fg mL^{-1} to 50 ng mL^{-1}	33.33 fg mL^{-1}	Tang et al. (2018)
Electrocatalysis of Pd/PCN-224-SA toward the oxidation of $NaBH_4$	DNA	100 fM to 100 nM	33.6 fM	Yan et al. (2018a)
Fe-MOFs/PdPt NPs bioconjugate to catalyze H_2O_2	Lead ions	0.005–1000 nM	2 pM	Yu et al. (2018)
PdNPs@Fe-MIL-88NH_2 for peroxidase-like activity of TMB	MicroRNA	0.01 fM to 10 pM	0.003 fM	Li et al. (2018b)
Electrocatalysis of Au@CeMOF toward HQ oxidation	Telomerase activity	2×10^2 to 2×10^6 cells mL^{-1}	27 cells mL^{-1}	Dong et al. (2019)
MOF-derived materials as effective immobilization matrixes of acetylcholinesterase	Methyl parathion	0.1 to 0.005 pg mL^{-1}	0.058 pg mL^{-1}	Dong et al. (2018)
Pd/NH_2-ZIF-67 as a carrier and synergistic catalyst to decompose H_2O_2	Prostate-specific antigen	100 fg mL^{-1} to 50 ng mL^{-1}	0.03 pg mL^{-1}	Dai et al. (2019)
Electrocatalytic activity of MOF-derived Ni_2P/graphene composites	Glucose	5 μM to 1.4 mM	0.44 μM	Zhang et al. (2018c)
CdS@ZIF-8 as signal tags by HCl leaching	*E. coli* O157:H7	10–10^8 CFU mL^{-1}	3 CFU mL^{-1}	Zhong et al. (2019)
Steric hindrance caused by the ZnZr bimetallic MOFs	Tyrosine kinase-7	0.001–1.0 ng mL^{-1}	0.84 pg mL^{-1}	Zhou et al. (2019)
Electroactive Co-MOFs as nanocarriers and signal labels to promote the oxidation of H_2O_2	Thrombin	1 pM to 30 nM	0.32 pM	Yang et al. (2017b)
ECL strategies				
Luminescence-functionalized Ru-MOF as ECL emitter	Tryptophan enantiomer	1.0 nM to 1.0 mM	0.33 nM	Zhu et al. (2017)
Dual-quenching ECL of $Ru(bpy)_3^{2+}$/zinc oxalate MOFs	Amyloid-β	100 fg mL^{-1} to 50 ng mL^{-1}	13.8 fg mL^{-1}	Zhao et al. (2019)
$Ru(bpy)_2(mcpbpy)^{2+}$ coordinated PCN-777	MUC1	100 fg mL^{-1} to 100 ng mL^{-1}	33.3 fg mL^{-1}	Hu et al. (2018)
Self-enhanced ruthenium polyethylenimine doped ZIF-8	Telomerase activity	5×10^1 to 10^6 Hela cells	11 cells	Xiong et al. (2017)
MoS_2 quantum dots-combined porphyrinic MOF-545	CEA	0.18–1000 ng mL^{-1}	0.45 pg mL^{-1}	Xin et al. (2018)
N-(aminobutyl)-N-(ethylisoluminol) functionalized Fe-MIL-101 as ECL indicator	Mucin1	1 fg mL^{-1} to 1 ng mL^{-1}	0.26 fg mL^{-1}	Jiang et al. (2017)
Co^{2+}-based ZIF-67 catalysis-enhanced luminol-AgNPs	Cardiac troponin I	1 fg mL^{-1} to 1 μg mL^{-1}	0.58 fg mL^{-1}	Wang et al. (2019a)
PEC strategies				
Charge recombination suppression strategy based on PCN-222	Phosphoprotein	0–2 μg mL^{-1}	0.13 μg mL^{-1}	Zhang et al. (2016b)
Efficient electron–hole separation of PCN-224/rGO nanocomposite	p-arsanilic acid	10 ng L^{-1} to 10 mg L^{-1}	5.47 ng L^{-1}	Peng et al. (2019)
Nitrogen-doped porous carbon-ZnO nanopolyhedra derived from ZIF-8	Alkaline phosphatase	2–1500 U L^{-1}	1.7 U L^{-1}	Yang et al. (2017a)
Synergistic effect of MOF-derived porous hollow carbon nanobubbles@ZnCdS cages	CEA	0.00005–500 ng mL^{-1}	2.28 fg mL^{-1}	Zhang et al. (2019)
Ru@UiO-66 sensitized Bi_2O_3/B–TiO_2/ITO	N^6-methyladenine	0.05–30 nM	0.0167 nM	Wang et al. (2019b)
$[Ru(bpy)_3]^{2+}$@UiO-66 probes as anchorages for phosphate groups and sensitizer	Kinase activity	0.005–0.0625 U mL^{-1}	0.0049 U mL^{-1}	Wang et al. (2017c)

structures, which exhibited the synergic effect to improve the biosensing performance. Fabrication of nanoparticle-functionalized MOFs (NP@MOFs) was usually divided into three different strategies: one-pot method to induce the NPs within the cavities of the MOF, post-absorption of NPs onto the MOF surfaces and in situ growth of MOF on pre-synthesized NPs (Bhardwaj et al., 2015; Wang et al., 2016b).

The in situ preparation of NP/MOFs benefits to the uniform distribution of NPs. Combining the benefits of both the nanoparticles and MOFs effectively, NP@MOFs have exhibited various application potentials in biosensing (Shen et al., 2018). For example, an electrochemical sensor based on electrocatalysis was constructed by one-pot encapsulation of platinum nanoparticles into a prototypal MOF for the detection of telomerase activity (Ling et al., 2016a). A MOF-based electroactive nanocomposite containing graphene fragments and HKUST-1 (Hong Kong University of Science and Technology-1) was synthesized via a facile one-step solvothermal method using GO, benzene-1,3,5-tricarboxylic acid (BTC), and copper nitrate ($Cu(NO_3)_2$) as the raw materials (Fig. 3A). Electrochemical assays showed that the synergy of graphene and HKUST-1 in the nanocomposite led to high electrocatalysis, fast response, and excellent selectivity toward the reduction of H_2O_2 (Wang et al., 2016a). These high analytical performances are attributed to the synergic effects of GO with the high conductivity and HKUST-1 MOF with suitable structure and electrochemical response. What's more, a Fe_3O_4/g-C_3N_4/HKUST-1 composite was synthesized by a solvothermal reaction, which combined HKUST-1 with g-C_3N_4 to improve its chemical stability (Hu et al., 2017).

Interestingly, the electrochemically driven cooperative reaction of $Ru(bpy)_3^{2+}$ as an ECL probe and structure-directing agent, trimesic acid as a ligand, and $Zn(NO_3)_2$ as the Zn^{2+} source led to a one-step and in situ synthesis and deposition of the MOF at a glassy carbon electrode surface. The Ru-MOF thin film modified electrode as a sensing platform showed excellent ECL behavior because massive $Ru(bpy)_3^{2+}$ molecules encapsulated in the cavity of the frameworks can be easily electrooxidated (Qin et al., 2018).

2.3. Post-modification of MOF structure

Usually, the immobilization of metal nanoparticles on frameworks through electrostatic adsorption can provide potential electrochemical candidates for biochemical sensor due to the strong catalysis sites, enlarged active surface area, and high conductivity. AuPt alloy doped hollow nanobox-MOFs were prepared as electroactive matrix toward the

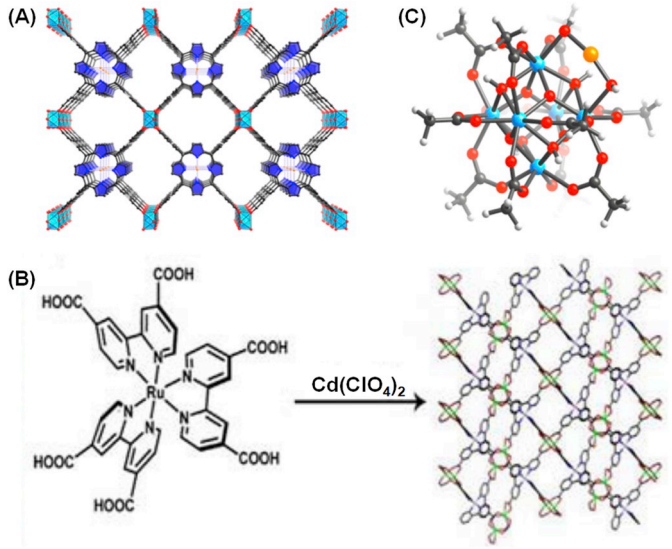

Fig. 2. (A) Illustration of the structure of a cobalt-porphyrin MOF, $Al_2(OH)_2TCPP\text{-}Co$ (reproduced from (Kornienko et al., 2015) with permission from The American Chemical Society), (B) the preparation of the Ru-MOF (reproduced from (Zhu et al., 2017) with permission from Elsevier), and (C) DFT calculated structure of a Cu/UiO-66 catalyst (reproduced from (Abdel--Mageed et al., 2019) with permission from The American Chemical Society).

reduction of H_2O_2 to yield an excellent electrochemical signal response (Xu et al., 2018a). Based on silver nanoclusters embedded UiO-66, an electrochemical biosensor was constructed with sensitive and selective detection capacity of trace carcinoembryonic antigen (CEA) (Guo et al., 2017).

As a mesoporous MOF featuring 3.8 nm cages, a porous coordination network (PCN)-777 is an ideal platform to incorporate functional molecular components through postsynthetic modification. The PCN-777 was chosen as the carrier to immobilize $Ru(bpy)_2(mcpbpy)^{2+}$ through the solvent-assisted ligand incorporation approach and successfully prepared a highly stable mesoporous luminescence-functionalized MOF (Ru–PCN-777) (Hu et al., 2018). The MOF UiO-66, constructed from $[Zr_6O_4(OH)_4]$ clusters with 1,4-benzenedicarboxylate struts has a high porosity that allows accommodation of various photosensitive molecules for PEC biosensor (Wang et al., 2019b).

To improve the conductivity, the calcining of MOFs is an efficient way. Among MOF-derived materials, the carbon matrix-supported metal oxide hybrid nanomaterials enable a high degree of homogenous dispersion of metal oxide species with large pore volume and superior conductivity. A series of metal ions, including Fe^{3+}, Zr^{4+}, and La^{3+}, were respectively connected with 2-aminoterephthalate to form three MOFs and then three MOF-derived materials were obtained by annealing them at 550 °C under N_2 atmosphere (Fig. 3B). These MOF-derived materials were all successfully used as effective immobilization matrixes of acetylcholinesterase to construct biosensors for the detection of methyl parathion (Dong et al., 2018). A CeO_{2-x}/C/reduced GO (rGO) nanocomposite has been synthesized through the pyrolysis of Ce(1,3,5-BTC) $(H_2O)_6$ with GO. The CeO_{2-x}/C/rGO nanocomposites exhibited excellent catalytic properties towards H_2O_2 due to the coexistence of Ce^{3+} and rGO (Peng et al., 2018). A unique "particle on a stick" approach was used to grow a single ZIF-67 nanoparticle on a nanoelectrode surface, and exhibited high catalytic activity toward the oxygen evolution reaction with a high turnover frequency of 29.7 s^{-1} at 540 mV overpotential (Aiyappa et al., 2019).

3. Electrochemical strategies

MOF's permanent porosity and high chemical stability enable their inherent superiority to confine guest species for improving catalytic performance and/or the expansion of reaction scope (Li et al., 2019). Especially, the rational integration of metal nanoparticles and MOFs effectively synergizes their respective strengths and offsets their drawbacks. Moreover, the long-term chemical stability of MOF in low pH environment and the protease resistance provided the protective cage around the encapsulated biomolecules for specific biorecognition (Feng et al., 2015; Lian et al., 2017). Thus, upon these advantages, a range of EC biosensors have been designed as expected.

3.1. Electrochemical/biomimetic catalysis

To develop porous MOFs as platforms for biomimetic catalysis, porphyrinic ligands have been extensively explored because of their multifunctionality. The rigid structures of porphyrinic MOF (PorMOF) with high surface area and porosity can not only make each porphyrin accessible by substrates but also prevent the dimerization of reaction centers. Apparently, the nanoscaled MOF material in the electrochemical biosensor could be more suitable as a signal transduction platform for electrocatalysis. By integrating the electrocatalysis of nanoscale PorMOF toward oxygen reduction and the telomerase triggered conformation switch, a simple and reliable strategy is developed for detection of telomerase activity (Ling et al., 2016b). The signal

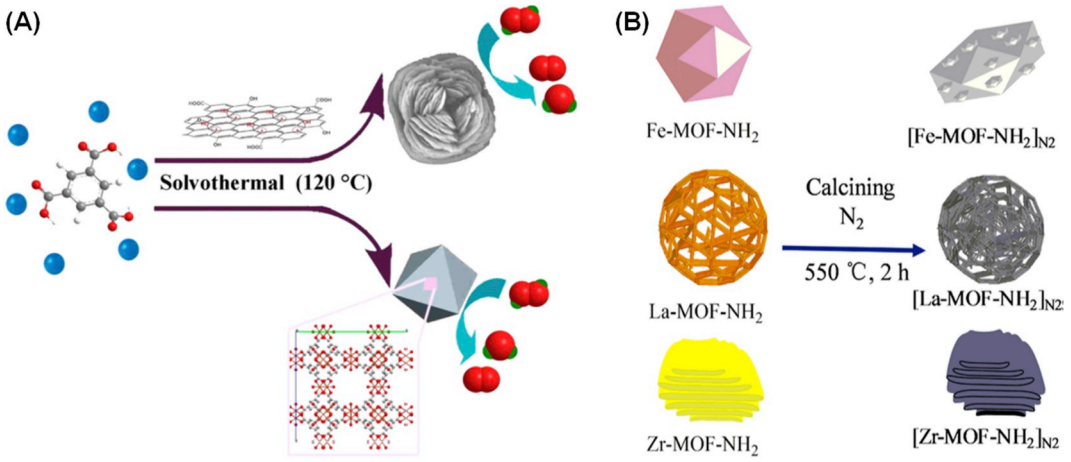

Fig. 3. (A) Illustration of the preparation of shaped GO@HKUST-1 and its application as a nonenzymatic electrocatalyst for H_2O_2 (reproduced from (Wang et al., 2016a) with permission from The American Chemical Society), and (B) the fabrication processes of three MOF-templated carbon nanocomposites (reproduced from (Dong et al., 2018) with permission from The American Chemical Society).

nanoprobe was prepared using porphyrin as linker and zirconium ion as node and sequentially functionalized with streptavidin (SA) as recognition element (Fig. 4). Afterward, through the biotin−streptavidin recognition, the PorMOF@SA nanoprobe was introduced to the electrode surface, leading to an enhanced current of electrocatalytic reduction toward oxygen for signal readout. The biosensor could detect telomerase with a detection limit of 30 cell mL^{-1} and evaluate the telomerase activity even in single HeLa cancer cell.

These porphyrin-based MOFs still have limited sensitivity in electrochemical assays because individual MOF regions suffer from slow charge transport. An integration of porphyrin-based MOFs into a conducting polymer would be a solution. A hybrid nanocomposite was proposed to synthesize by composing a conductive polymer poly(3,4-ethylenedioxythiophene) with porphyrin-based MOF-525 nanocrystal. Interestingly, the MOF-525 served as an electrocatalytic surface, while the polymer acted as a charge collector to rapidly transport the electron from MOF nanocrystals (Huang et al., 2017). The composite electrode also exhibited excellent selectivity for dopamine against common interferents and retained long-term sensing ability.

Due to the tunable pore voids and functional pore walls, MOF provides a new opportunity for mimetic catalysis. In fact, a carbon paste electrode modified with a MIL-101(Fe) exhibited high electrocatalysis toward citric acid oxidation, and was successfully applied to the determination of citric acid in commercial beverages (Valizadeh et al., 2019). The ultrathin Ni–Co MOF sheets were reported to efficiently catalyze oxygen evolution reaction with high turnover frequency (0.86 s^{-1}) at low onset potential (Zhao et al., 2016). Moreover, a series of iron porphyrin derivatives can be readily functionalized as suitable components for the construction of MOFs, showing interesting peroxidase activity comparable to that of the heme protein. For example, a porphyrin-encapsulated MOF material was achieved through a one-pot incorporation of porphyrin into the cage of HKUST-1(Cu) as catalyst. By coupling with peroxidase activity of porphyrin-encapsulated MOF toward o-phenylenediamine (o-PD) oxidation in the presence of H_2O_2, a label-free electrochemical strategy for DNA detection was designed through the allosteric switch of hairpin DNA (Fig. 5A). The "signal-on" electrochemical sensor can detect target DNA down to 0.48 fM with the linear range of 10 fM to 10 nM (Ling et al., 2015). This strategy opens up a new direction of porphyrin-functionalized MOF for signal transduction in electrochemical biosensing.

Furthermore, an AuNP@PorMOF signal tag was designed by using porphyrin as linkers and Fe^{3+} as nodes, and then the AuNPs were immobilized on the surface of MOF through animation of silicon dioxide. Based on the peroxidase-like catalytic performance of AuNP@PorMOF for oxidation of 3,3′,5,5′-tetramethylbenzidine (TMB) by H_2O_2 (Fig. 5B), a highly sensitive electrochemical biosensor combined with a 3D origami device for detection of Pb^{2+} was developed (Wang et al., 2017b). This method showed a good linear relationship between the current response and the Pb^{2+} concentration ranging from 0.03 to 1000 nM with a detection limit of 0.02 nM, providing potential application of real-time Pb^{2+} detection in both environmental and biological samples. In our group, a ratiometric electrochemical technique was constructed based on the catalytic properties of MOFs toward hydroquinone oxidation to p-benzoquinone and the electroactive methylene blue-labeled hairpin DNA for rapid and sensitive detection of telomerase activity (Dong et al., 2019).

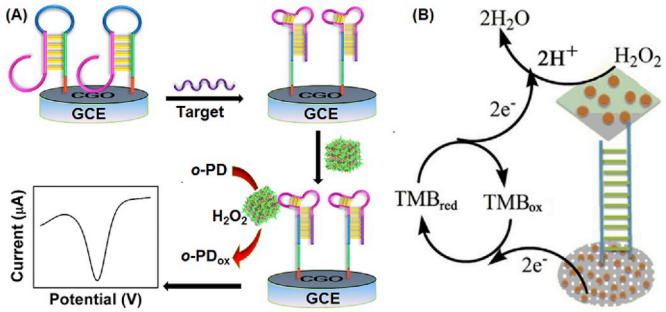

Fig. 5. (A) FeTCPP@MOF-SA composite for electrochemical DNA sensing via allosteric switch of hairpin DNA (reproduced from (Ling et al., 2015) with permission from The American Chemical Society), and (B) Peroxidase-like catalytic performance of AuNP@PorMOF toward TMB oxidation (reproduced from (Wang et al., 2017b) with permission from Elsevier).

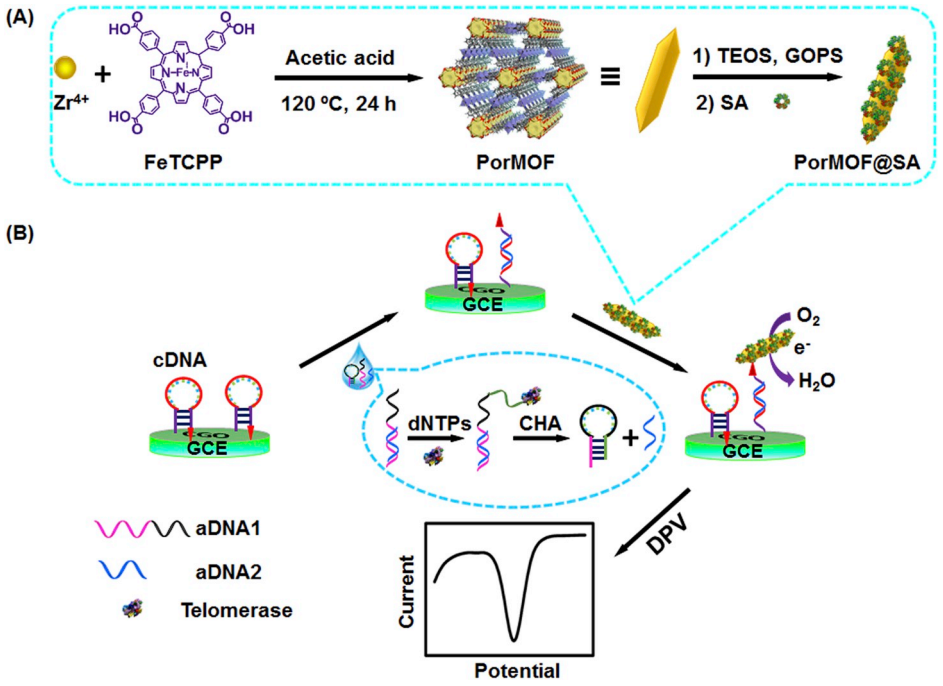

Fig. 4. Schematic illustration of (A) the preparation of nanoscaled PorMOF and (B) the electrochemical detection strategy for telomerase activity via a telomerase triggered conformation switch (reproduced from (Ling et al., 2016b) with permission from The American Chemical Society).

3.2. MOFs as supporters and nanocontainers

Due to the porous properties, the MOFs can load large amount of electroactive molecules for enhancing the electrochemical performance. For example, a Pd/PCN-224-SA as signal tag was synthesized by in situ reduction of Pd nanocrystals on porphyrinic metal−organic frameworks (PCN-224), followed by conjugation with SA. By integrating signal amplification of DNA walker, the electrocatalysis of Pd/PCN-224-SA tag toward $NaBH_4$ oxidation was used to produce a large electrochemical signal for DNA analysis (Fig. 6). The electrochemical biosensor demonstrated an excellent detection performance such as 6 orders of magnitude linear range, femtomolar detection limit, and single mismatch differentiation ability. The tandem signal amplification of MOFs and DNA walkers provided a new avenue in trace electrochemical biosensing (Yan et al., 2018a). Since the electroactive ZIF-67 with lamellar structures served not only as a carrier of Pd NPs but also as a synergistic catalyst of palladium to decompose H_2O_2, the Pd/NH_2-ZIF-67 nanocomposite was conducted to achieve the quantitative determination of prostate specific antigen (PSA), featuring favorable selectivity, repeatability and stability (Dai et al., 2019).

Owing to their periodic topology structure, variable metal site, and tunable open-framework, MOFs have been considered as ideal precursors for synthesizing metal compounds with porous structures. Interestingly, an efficient and facile MOF-template strategy for preparing carbon nanocomposites has been developed. With Ni-MOF-74 as a precursor, Ni_2P nanoparticles were grown in situ on graphene (Ni_2P/G), and showed even metal distribution, massive exposure of active sites, and spatially ordered structure. Benefiting from the synergistic reaction of Ni_2P particles and graphene, this MOF-derived composite exhibited high electrocatalytic activity and specificity toward glucose electrooxidation with a detection limit of 0.44 μM (Zhang et al., 2018c). Ni-MOF/Ni/NiO/carbon frame nanocomposite was formed by combing Ni and NiO nanoparticles and a C frame with Ni-MOF using an efficient one-step calcination method. Ni-MOF/Ni/NiO/C nanocomposites were immobilized onto glassy carbon electrodes with Nafion film to construct high-performance nonenzymatic glucose and H_2O_2 electrochemical sensors (Shu et al., 2017).

Furthermore, it is well established that MOFs could be used as nanocarriers to encapsulate organic molecules and release them through specific stimuli. When MOFs was introduced into a homogeneous electrochemical biosensor, such a developed biosensor not only avoids the drawback of weak conductivity but also achieves the label-free and enzyme-free ultrasensitive detection of target analytes. Typically, a nucleic acid-functionalized MOF-based homogeneous electrochemical strategy was established with label-free and enzyme-free features for ultrasensitive and simultaneous detection of multiple tumor biomarkers (Chang et al., 2019). The two functionalized MOFs (MB@UIO and TMB@UIO) were fabricated by using porous UIO-66-NH_2 as nanocontainer to load electroactive dyes and double-strand DNA as a gatekeeper to cap MOFs (Fig. 7). The proposed DNA-capped MOFs showed specific response toward target analytes based on target-initiated electroactive dye release, and were applied to simultaneous detection of let-7a and miRNA-21 with detection limits down to 3.6 and 8.2 fM, respectively. Therefore, the proposed strategy was expected to provide more information for early and accurate cancer diagnosis.

In addition, based on the blocking effect of MOFs, a ZnZr bimetallic MOF was prepared via the MOF-on-MOF method and exploit it as an aptasensor platform for detecting the cancer marker protein tyrosine kinase-7 (Zhou et al., 2019). Next, a nanohybird of Co-based MOF and terephthalonitrile-based covalent organic framework was synthesized,

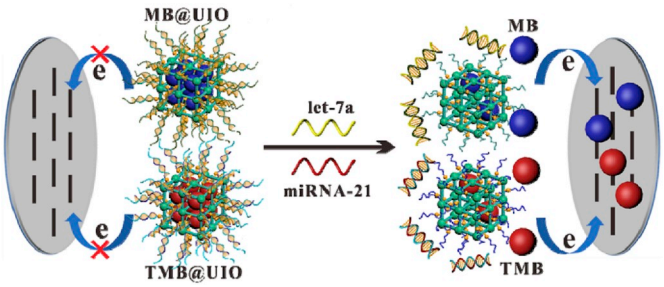

Fig. 7. Schematic representation of the principle of the MOF-based homogeneous electrochemical biosensor for multiple detection of miRNAs (reproduced from (Chang et al., 2019) with permission from The American Chemical Society).

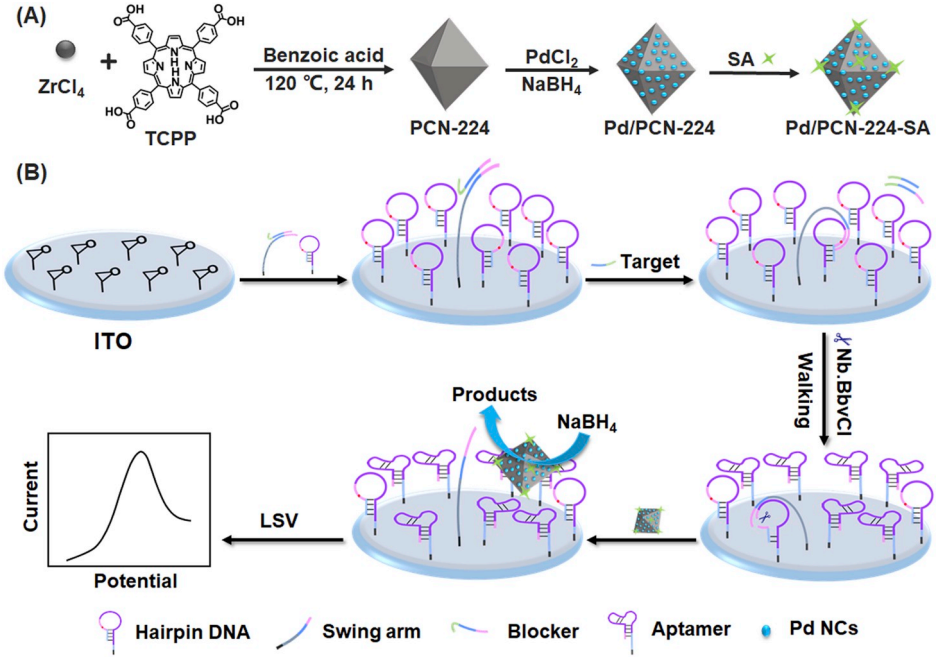

Fig. 6. Schematic illustration of (A) synthesis of Pd/PCN-224-SA tags and (B) tandem signal amplification strategy based on DNA-walker-induced allosteric switch and electrocatalysis of Pd/PCN-224-SA in electrochemical biosensing (reproduced from (Yan et al., 2018a) with permission from The American Chemical Society).

and further explored its application in constructing a sensitive electrochemical aptasensor for ampicillin detection (Liu et al., 2019b). Compared with MOFs containing divalent d-block metals, trivalent Al (III) MOFs with high specific surface area and physicochemical stability provided a universal platform in designing desired electrochemical biosensors (Liu et al., 2017). Interestingly, the reaction of Fe^{3+} in the MOF with $K_4Fe(CN)_6$ led to the formation of prussian blue on the electrode surface and consequently the generation of a high electrochemical signal, which achieved great signal amplification without the involvement of any extra functional materials (Cui et al., 2018).

4. ECL strategies

Different from the conventional emitters, the MOF-based ECL emitters can accelerate the electron transfer between ECL emitters and coreactants due to their porous structures, and thus enhance the performance of ECL biosensing. In particular, Ru(II) ploypyridyl (Rubpy) complexes are of specific interest in the synthesis of various MOF-based ECL emitters, which can combine their merits together. The Rubpy complexes usually, as the guest molecules, have been doped in the frameworks and/or encapsulated in the pores of MOFs. For example, the ECL-active MOF was prepared from $\{Ru[4,4'\text{-}(HO_2C)_2\text{-}bpy]_2bpy\}^{2+}$ and Zn^{2+} (Fig. 8A). The designed MOF exhibited permselectivity, charge selectivity, and catalytic selectivity along with a stable and concentration-dependent ECL emission due to the ease of electron transfer between the MOF and coreactants. The detection and recovery of cocaine in the serum sample was used to validate the feasibility of MOF-based ECL system (Xu et al., 2015). Based on CdS QDs as coreactant, a luminescence-functionalized Ru-MOF nanoflower was employed as a solid-state ECL "on-off" switch system for highly sensitive detection of tryptophan (Zhu et al., 2017). Inspired by the 2D nanomaterials g-C_3N_4@AuNPs and Ru-MOF that could exhibit two strong and stable ECL emissions at different potentials, a potential-resolved Faraday cage-type ECL biosensor was designed and constructed for the simultaneous detection of miRNA-141 and miRNA-21 (Shao et al., 2018a).

Alternatively, a mesoporous luminescence-functionalized MOF (Ru–PCN-777) was synthesized by immobilizing Ru-$(bpy)_2(mcpbpy)^{2+}$ on the Zr_6 cluster of PCN-777 via a strong coordination bond between Zr^{4+} and –COO– (Fig. 8B). Consequently, the $Ru(bpy)_2(mcpbpy)^{2+}$ was not only covered on the surface of PCN-777 but also grafted into the interior of PCN-777, which greatly increased the loading amount of Ru $(bpy)_2(mcpbpy)^{2+}$. Because of the mesoporosity of Ru–PCN-777, the Ru $(bpy)_2(mcpbpy)^{2+}$ on the surface and interior of Ru–PCN-777 could be excited by the electrons, resulting in the increasing utilization ratio of the $Ru(bpy)_2(mcpbpy)^{2+}$ to enhance the high ECL response (Hu et al., 2018). Compared with 3D bulk MOFs, ultrathin metal-organic layer (MOL) could immobilize luminophores for effectively shortening the ion/electron-transport distance and relieving the diffusional constraints of ion/electron. Thus, the Hf-MOL was prepared as carrier to immobilize $Ru(bpy)_2(mcpbpy)^{2+}$, and the ECL efficiency and intensity of Ru-Hf-MOL were around 1.27 times and 14.5 times than those of Ru–PCN-777, respectively (Hu et al., 2019). In the same group, a self-enhanced ECL aptasensor utilizing Ru complex-grafted Zr-MOL as an ECL tag was also developed for ultrasensitive Mucin 1 analysis (Yang et al., 2019). Similarly, an ultrasensitive "off−on" ECL biosensor was proposed for the determination of telomerase activity by using a self-enhanced ruthenium polyethylenimine complex doped ZIF-8 as an ECL indicator and an enzyme-assisted DNA cycle amplification strategy (Xiong et al., 2017).

Metal nodes in MOF can accelerate the decomposition of reactant H_2O_2 to generate $OH^{\bullet}$, $O_2^{\bullet-}$, and other radical derivatives for enhancing the ECL performance of the luminol system. Luminol-capped AgNPs (luminol-AgNPs) were decorated on the surface of ZIF-67 by electrostatic interaction (Fig. 8C). Because of the ordered crystalline structure, porosity, and the atomically dispersed Co^{2+}, the integrated MOF-based luminol nanosystem can facilitate the generation of oxygen radicals and greatly improve its ECL performance (with ~115-fold enhancement). On the basis of this fascinating sensing platform, a label-free ECL immunosensor was constructed for ultrasensitive detection of cardiac troponin I, the main marker of myocardial infarction, with good stability and a detection limit as low as 0.58 fg mL^{-1} (Wang et al., 2019a). It is worth noting that the ECL signal of luminol derivate/MIL-101(Fe) could be greatly heightened due to the intrinsic mimic peroxidase activity of luminol derivate/MIL-101(Fe) that could accelerate the decomposition of H_2O_2 and produce considerable numbers of reactive oxygen radicals to participate in the ECL reaction of luminol derivate (Wang et al., 2018b). A sensitive ECL biosensor for protein kinase A activity analysis was proposed based on bimetallic catalysis of Au and Pt nanoparticles on AuPt@UiO-66 nanocomposite to enhance luminol emission (Yan et al., 2018b). Interestingly, based on Fe-MIL-88 MOF/Au NPs/G-quadruplex as both quenchers and enhancers, a ratiometric ECL aptasensor exhibited high-sensitive and accurate analytical performance toward PSA with a linear detection range from 0.5 to 500 ng mL^{-1} (Shao et al., 2018b).

ECL behaviours involving oxygen molecules have been previously reported. The photoelectric active groups zinc tetrakis(carboxyphenyl)-porphyrin (ZnTCPP) on the MOF-525-Zn frameworks could promote the generation of singlet oxygen via a series of electrochemical and chemical reactions, resulting in a strong and stable red irradiation at 634 nm (Zhang et al., 2016a). The MOF-545-Zn@QDs was feasibly prepared with the ultrasonic method through the interaction between MoS_2 QDs

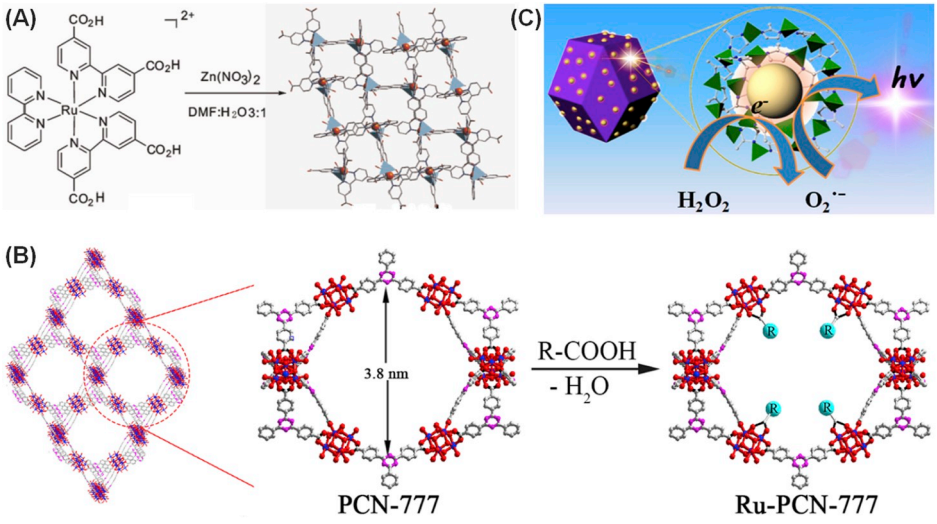

Fig. 8. (A) Preparation of redox-active MOF from $\{Ru[4,4'\text{-}(HO_2C)_2\text{-}bpy]_2bpy\}^{2+}$ and Zn^{2+} (reproduced from (Xu et al., 2015) with permission from Elsevier), (B) Schematic depiction of incorporating $Ru(bpy)_2(mcpbpy)^{2+}$ inside the channels of PCN-777 through the solvent-assisted ligand incorporation approach (reproduced from (Hu et al., 2018) with permission from The American Chemical Society), and (C) Schematic illustration of the integration of Co-based MOF and AgNPs for the enhancement of luminol ECL (reproduced from (Wang et al., 2019a) with permission from The American Chemical Society).

and MOF-545-Zn. The MoS_2 QDs increased ECL intensity of MOF-545-Zn because of the O_2 enrichment and electron transformation (Xin et al., 2018).

Resonance energy transfer is a powerful method for monitoring particular target molecules in fluorescence and ECL, which depends on the overlap of absorption and emission spectral, as well as the distance (10 ± 2 nm) between the energy donor and acceptor. Inspired by this thought, an ECL resonance energy transfer strategy between AuNPs–doped MOF and $Ru(bpy)_3^{2+}$/silica nanoparticle was reported for the determination of insulin (Ma et al., 2016). For example, a gears ECL aptasensing strategy for multiple selective determination of kanamycin and neocycin was designed on the basis of MIL-53(Fe)@CdS as the ECL luminophores and nanostructural metallic (AuNPs or PtNPs) functioning as both ECL quencher and enhancer (Feng et al., 2019). A dual-quenching ECL immunosensor based on $Ru(bpy)_3^{2+}$/zinc oxalate MOFs as luminophor and Au@NiFe MOFs as the dual quencher was constructed for the ultrasensitive detection of amyloid-β (Zhao et al., 2019).

5. PEC strategies

PEC is a promising analytical technique that employs current as a detection signal with light as an excitation source. Thus, the PEC detection possesses potentially high sensitivity and reduced background signals compared with conventional electrochemical and optical methods. For the PEC analysis, photoactive material plays a very important role in improving the photoelectric conversion efficiency and obtaining desirable analytical performance. Except for the conventional photoactive material such as metal oxide semiconductors, the MOF composites have anticipant structure used to construct PEC sensors. In particular, porphyrinic MOFs, constructed from porphyrinic or metalloporphyrinic ligands, have attracted continuous research interest based on the remarkable features, such as the small valence band (HOMO)-conduction band (LUMO) energy gap of porphyrinic MOFs and the prolonged electron−hole recombination time within the framework, which can enhance the photoelectric conversion efficiency. For example, the TCPP ligand involving PCN-222 is able to act as a visible light-harvesting unit, and the high porosity and tunable structures might facilitate the enrichment of oxygen and dopamine (DA) molecules around the PEC-active TCPP ligands. Under light irradiation, the TCPP in PCN-222 behaved as a visible-light-harvesting unit, and electrons transformed from HOMO to LUMO of the semiconductor-like PCN-222, and generated electron−hole pairs. Then electrons transformed from LUMO of PCN-222 to O_2 to produce $O_2^{\bullet-}$, realizing the electron circuit and thereby enhancing the photoelectric conversion efficiency (Zhang et al., 2016b). Based on the steric hindrance effect from the coordination of the phosphate groups and inorganic Zr–O clusters as binding sites in PCN-222, the PCN-222 modified electrode could be applied for the label-free detection of phosphoproteins with the limit of detection down to 0.13 μg mL^{-1} (Fig. 9A). Based on the DNA-mediated nanoscale zirconium-porphyrin MOFs, an enzyme-free PEC immunoassay was developed for the ultrasensitive detection of PSA (Zhang et al., 2018a). Furthermore, a porphyrinic MOF/reduced grapheme oxide (PCN-224/rGO) nanocomposite with simultaneously excellent photoelectric activity and strong binding characteristics was prepared and used to fabricate a PEC sensor for *p*-arsanilic acid detection avoiding the modification of bio-recognizers (Peng et al., 2019).

A turn-on PEC biosensor based on the surface defect recognition and multiple signal amplification of MOFs was proposed for highly sensitive protein kinase activity analysis and inhibitor evaluation (Wang et al., 2017c). In this strategy, based on the phosphorylation reaction in the presence of protein kinase A, the Zr-based MOFs (UiO-66) accommodated with $[Ru(bpy)_3]^{2+}$ photoactive dyes in the pores were linked to the phosphorylated kemptide modified TiO_2/ITO electrode through the chelation between the Zr^{4+} defects on the surface of UiO-66 and the phosphate groups in kemptide (Fig. 9B). Under visible light irradiation, the excited electrons from $[Ru(bpy)_3]^{2+}$ adsorbed in the pores of UiO-66 were injected into the TiO_2 CB to generate photocurrent, affording a highly sensitive PEC analysis of kinase activity. Interestingly, ZnO@ZIF-8 core−shell heterostructures display distinct PEC response to hole scavengers with different molecule sizes (e.g., H_2O_2 and ascorbic acid) owing to the limitation of the aperture of the ZIF-8 shell. Such ZnO@ZIF-8 nanorod arrays were successfully applied to the detection of H_2O_2 in the presence of serous buffer solution (Zhan et al., 2013).

To improve the electrical conductivity of MOFs and to make better for their applications in PEC sensor. A photoactive material, nitrogen-doped porous carbon-ZnO (NPC–ZnO) nanopolyhedra, was prepared by direct carbonization of ZIF-8 nanopolyhedra in a nitrogen atmosphere. The interaction between NPC and ZnO may change the band gap of ZnO and broaden the light absorption range from ultraviolet to visible light, showing better PEC performance than ZnO nanorod and the ZIF-8 nanopolyhedra in aqueous media with dissolved oxygen and ascorbic acid (Fig. 9C). Taking alkaline phosphatase as a model, a NPC-ZnO nanopolyhedra-based PEC sensor showed good performance for alkaline phosphatase assay with a wide linear response range from 2 to 1500 U L^{-1} and a low detection limit of 1.7 U L^{-1} (Yang et al., 2017a). Interestingly, as novel photoactive materials, MOF-derived porous hollow carbon nanobubbles@ZnCdS multi-shelled dodecahedral cages

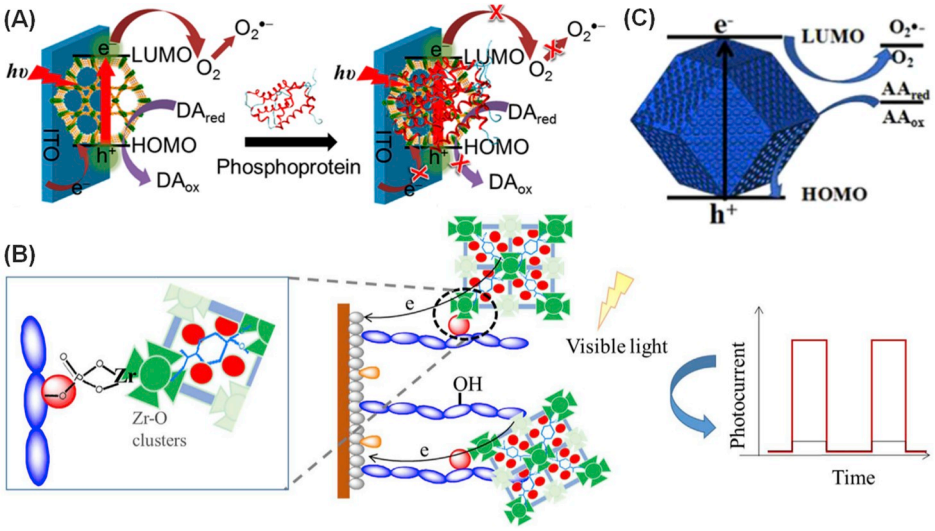

Fig. 9. Schematic illustration for (A) the mechanism of charge recombination suppression-based photoelectrochemical strategy for the detection of phosphoprotein (reproduced from (Zhang et al., 2016b) with permission from The American Chemical Society), (B) the configuration of $[Ru(bpy)_3]^{2+}$@UiO-66 PEC probe for kinase activity detection (reproduced from (Wang et al., 2017c) with permission from Elsevier), and (C) the cathodic photocurrent generation mechanism of the ITO/NPC-ZnO electrode (reproduced from (Yang et al., 2017a) with permission from The American Chemical Society).

were synthesized via continuous chemical etching, sulfurization, cation-exchange and calcination strategies. Due to the synergistic effect between the porous shells and the carbon-layer coating, the MOF-derived composite displayed superior PEC performance (Zhang et al., 2019).

6. Conclusion and future perspectives

MOFs have become a promising candidate to immobilize various nanoparticle and/or biomolecules owing to the modular nature and mild synthesis conditions (Baek et al., 2018). There are three different strategies to modify MOFs easily for the great potential in electrochemical application: dopant modification, in situ entrapping functional molecules or nanoparticles within the framework, and post-modification methods. To facilitate the applications of MOFs in electrochemical biosensing, the current researches mainly focused on the functionalization of MOFs with the electroactive nanoparticles/biomolecules. By integrating functional materials at nanometer scale, MOF heterogeneous nanohybrids demonstrated the collective properties for designing an ideal sensing platforms (Diercks et al., 2018): (i) MOFs' porous structures make all the active sites accessible and their open channels render the diffusion of the substrate and products easily; (ii) The high surface area of MOFs materials is beneficial to enable novel EC systems and protocols due to the increasing areal density of electroactive sites; (iii) MOF-based hybrid materials with other functional materials greatly improve the conductivity of MOFs and exhibit the synergic effect among individual components for signal transduction in electrochemical biosensors.

Actually, the research on electroactive MOF-based biosensors is at an initial stage. For example, only few MOF structures are involved in the fields of electrochemical biosensing. To further expand its application and enhance its sensing performance, some aspects should be explored for further work: (1) One of the challenges for MOF-based EC systems is the design of redox-active ligands such as aggregation-induced emission molecules and Ru nodes in MOFs with high electron transfer capacities and electrocatalytic ability, for enhancing the electrochemical performance; (2) the 2D MOF's immobilization amount of electroactive species should be higher than these of bulk MOFs because MOLs possess more accessible postmodification sites for the electroactive species with minimal diffusion barriers (Córdova Wong et al., 2019); (3) Utilization of MOFs as templates to synthesize metal oxide/carbon nanocomposites is a facile and efficient method to improve the electrochemical performance of MOF composites; (4) MOFs are often transparent single crystals, which allow for light to penetrate through the whole materials, and thus give the great potential for developing ECL and PEC biosensing; (5) By combination of several emerging techniques, the great progress and major technological breakthroughs can be achieved in current and future work. For example, the core-shell MOF@MOF and MOF@covalent organic frameworks could enable the new properties for enhancing their sensing applications (Ma, et al., 2018). In a word, with the rational design and post-modification, the MOF composites could be more suitable as a signal transduction platform for electrochemical biosensing with a wide range of applications in disease monitoring and clinical diagnosis.

Declaration of competing interest

The authors declare that they have no known competing financial interests or personal relationships that could have appeared to influence the work reported in this paper.

CRediT authorship contribution statement

Xianjiu Liao: Writing - original draft. **Jianping Lei:** Writing - original draft, Supervision, Investigation.

Acknowledgments

We gratefully acknowledge the National Natural Science Foundation of China (21605082, 21675084, 21665026), Distinguished Young Talents of Youjiang Medical University for Nationalities, and Guangxi Clinic Medicine Research Center of Hepatobiliary Diseases (AD17129025).

References

Abdel-Mageed, A.M., Rungtaweevoranit, B., Parlinska-Wojtan, M., Pei, X.K., Yaghi, O.M., Behm, R.J., 2019. J. Am. Chem. Soc. 141, 5201–5210.
Aiyappa, H.B., Wilde, P., Quast, T., Masa, J., Andronescu, C., Chen, Y.T., Muhler, M., Fischer, R.A., Schuhmann, W., 2019. Angew. Chem. Int. Ed. 58, 8927–8931.
Baek, J., Rungtaweevoranit, B., Pei, X.K., Park, M., Fakra, S.C., Liu, Y.S., Matheu, R., Alshmimri, S.A., Alshehri, S., Trickett, C.A., Somorjai, G.A., Yaghi, O.M., 2018. J. Am. Chem. Soc. 140, 18208–18216.
Bhardwaj, S.K., Bhardwaj, N., Mohanta, G.C., Kumar, P., Sharma, A.L., Kim, K.H., Deep, A., 2015. ACS Appl. Mater. Interfaces 7, 26124–26130.
Chang, J.F., Wang, X., Wang, J., Li, H.Y., Li, F., 2019. Anal. Chem. 91, 3604–3610.
Cho, H.S., Yang, J.J., Gong, X., Zhang, Y.B., Momma, K., Weckhuysen, B.M., Deng, H.X., Kang, J.K., Yaghi, O.M., Terasaki, O., 2019. Nat. Chem. 11, 562–570.
Córdova Wong, B.J., Xu, D.M., Bao, S.S., Zheng, L.M., Lei, J.P., 2019. ACS Appl. Mater. Interfaces 11, 12986–12992.
Cui, L., Hu, J., Li, C.C., Wang, C.M., Zhang, C.Y., 2018. Biosens. Bioelectron. 122, 168–174.
Dai, H.X., Lü, W.J., Zuo, X.W., Zhu, Q., Pan, C.J., Niu, X.Y., Liu, J.J., Chen, H.L., Chen, X. G., 2017. Biosens. Bioelectron. 95, 131–137.
Dai, L., Li, Y.Y., Wang, Y.G., Luo, X.L., Wei, D., Feng, R., Yan, T., Ren, X., Du, B., Wei, Q., 2019. Biosens. Bioelectron. 132, 97–104.
Diercks, C.S., Liu, Y.Z., Cordova, K.E., Yaghi, O.M., 2018. Nat. Mater. 17, 301–307.
Dolgopolova, E.A., Rice, A.M., Martin, C.R., Shustova, N.B., 2018. Chem. Soc. Rev. 47, 4710–4728.
Dong, P.F., Zhu, L.Y., Huang, J., Ren, J.J., Lei, J.P., 2019. Biosens. Bioelectron. 138, 111313.
Dong, S.Y., Peng, L., Wei, W.B., Huang, T.L., 2018. ACS Appl. Mater. Interfaces 10, 14665–14672.
Feng, D.F., Tan, X.C., Wu, Y.Y., Ai, C.H., Luo, Y.N., Chen, Q.Y., Han, H.Y., 2019. Biosens. Bioelectron. 129, 100–106.
Feng, D.W., Liu, T.F., Su, J., Bosch, M., Wei, Z.W., Wan, W., Yuan, D.Q., Chen, Y.P., Wang, X., Wang, K.C., Lian, X.Z., Gu, Z.Y., Park, J., Zou, X.D., Zhou, H.C., 2015. Nat. Commun. 6, 5979.
Guo, C.P., Su, F.F., Song, Y.P., Hu, B., Wang, M.H., He, L.H., Peng, D.L., Zhang, Z.H., 2017. ACS Appl. Mater. Interfaces 9, 41188–41199.
Hassanzadeh, J., Khataee, A., Eskandari, H., 2018. Sens. Actuators B Chem. 259, 402–410.
Hu, G.B., Xiong, C.Y., Liang, W.B., Yang, Y., Yao, L.Y., Huang, W., Luo, W., Yuan, R., Xiao, D.R., 2019. Biosens. Bioelectron. 135, 95–101.
Hu, G.B., Xiong, C.Y., Liang, W.B., Zeng, X.S., Xu, H.L., Yang, Y., Yao, L.Y., Yuan, R., Xiao, D.R., 2018. ACS Appl. Mater. Interfaces 10, 15913–15919.
Hu, S.S., Ouyang, W.J., Guo, L.H., Lin, Z.Y., Jiang, X.H., Qiu, B., Chen, G.N., 2017. Biosens. Bioelectron. 92, 718–723.
Huang, T.Y., Kung, C.W., Liao, Y.T., Kao, S.Y., Cheng, M.S., Chang, T.H., Henzie, J., Alamri, H.R., Alothman, Z.A., Yamauchi, Y., Ho, K.C., Wu, K.C.W., 2017. Adv. Sci. 4, 1700261.
Jiang, X.Y., Wang, Z.L., Wang, H.J., Zhuo, Y., Ruo, Y., Chai, Y.Q., 2017. Chem. Commun. 53, 9705–9708.
Kempahanumakkagari, S., Vellingiri, K., Deep, A., Kwon, E.E., Bolan, N., Kim, K.H., 2018. Coord. Chem. Rev. 357, 105–129.
Koo, W.T., Choi, S.J., Kim, S.J., Jang, J.S., Tuller, H.L., Kim, I.D., 2016. J. Am. Chem. Soc. 138, 13431–13437.
Kornienko, N., Zhao, Y.B., Kley, C.S., Zhu, C.H., Kim, D., Lin, S., Chang, C.J., Yaghi, O.M., Yang, P.D., 2015. J. Am. Chem. Soc. 137, 14129–14135.
Kozachuk, O., Luz, I., Llabrés i Xamena, F.X., Noei, H., Kauer, M., Albada, H.B., Bloch, E. D., Marler, B., Wang, Y.M., Muhler, M., Fischer, R.A., 2014. Angew. Chem. Int. Ed. 53, 7058–7062.
Li, B., Wen, H.M., Cui, Y.J., Zhou, W., Qian, G.D., Chen, B.L., 2016. Adv. Mater. 28, 8819–8860.
Li, G.D., Zhao, S.L., Zhang, Y., Tang, Z.Y., 2018. Adv. Mater. 30, 1800702.
Li, P., Zeng, H.C., 2016. ACS Appl. Mater. Interfaces 8, 29551–29564.
Li, Y.L., Yu, C., Yang, B., Liu, Z.R., Xia, P.Y., Wang, Q., 2018. Biosens. Bioelectron. 102, 307–315.
Li, Y.Z., Fu, Z.H., Xu, G., 2019. Coord. Chem. Rev. 388, 79–106.
Lian, X.Z., Erazo-Oliveras, A., Pellois, J.P., Zhou, H.C., 2017. Nat. Commun. 8, 2075.
Ling, P.H., Lei, J.P., Jia, L., Ju, H.X., 2016. Chem. Commun. 52, 1226–1229.
Ling, P.H., Lei, J.P., Ju, H.X., 2016. Anal. Chem. 88, 10680–10686.
Ling, P.H., Lei, J.P., Zhang, L., Ju, H.X., 2015. Anal. Chem. 87, 3957–3963.
Ling, P.H., Qian, C.H., Gao, F., Lei, J.P., 2018. Chem. Commun. 54, 11176–11179.
Liu, C.S., Sun, C.X., Tian, J.Y., Wang, Z.W., Ji, H.F., Song, Y.P., Zhang, S., Zhang, Z.H., He, L.H., Du, M., 2017. Biosens. Bioelectron. 91, 804–810.
Liu, J.T., Liu, T.R., Du, P., Zhang, L., Lei, J.P., 2019. Angew. Chem. Int. Ed. 58, 7808–7812.

Liu, T.Z., Hu, R., Zhang, X., Zhang, K.L., Liu, Y., Zhang, X.B., Bai, R.Y., Li, D.L., Yang, Y. H., 2016. Anal. Chem. 88, 12516–12523.
Liu, X.K., Hu, M.Y., Wang, M.H., Song, Y.P., Zhou, N., He, L.H., Zhang, Z.H., 2019. Biosens. Bioelectron. 123, 59–68.
Lu, G., Li, S.Z., Guo, Z., Farha, O.K., Hauser, B.G., Qi, X.Y., Wang, Y., Wang, X., Han, S.Y., Liu, X.G., DuChene, J.S., Zhang, H., Zhang, Q.C., Chen, X.D., Ma, J., Loo, S.C.J., Wei, W.D., Yang, Y.H., Hupp, J.T., Huo, F.W., 2012. Nat. Chem. 4, 310–316.
Lu, K.D., Aung, T., Guo, N.N., Weichselbaum, R., Lin, W.B., 2018. Adv. Mater. 30, 1707634.
Lu, K.D., He, C.B., Guo, N.N., Chan, C., Ni, K.Y., Lan, G.X., Tang, H.D., Pelizzari, C., Fu, Y. X., Spiotto, M.T., Weichselbaum, R.R., Lin, W.B., 2018. Nat. Biomed. Engin. 2, 600–610.
Ma, H.M., Li, X.J., Yan, T., Li, Y., Liu, H.Y., Zhang, Y., Wu, D., Du, B., Wei, Q., 2016. ACS Appl. Mater. Interfaces 8, 10121–10127.
Ma, T.Q., Kapustin, E.A., Yin, S.X., Liang, L., Zhou, Z.Y., Niu, J., Li, L.H., Wang, Y.Y., Su, J., Li, J., Wang, X.G., Wang, W.D., Wang, W., Sun, J.L., Yaghi, O.M., 2018. Science 361, 48–52.
Ma, W.J., Jiang, Q., Yu, P., Yang, L.F., Mao, L.Q., 2013. Anal. Chem. 85, 7550–7557.
Mao, D., Hu, F., Kenry Ji, S.L., Wu, W.B., Ding, D., Kong, D.L., Liu, B., 2018. Adv. Mater. 30, 1706831.
Micheroni, D., Lan, G.X., Lin, W.B., 2018. J. Am. Chem. Soc. 140, 15591–15595.
Pan, Y., Sun, K.A., Liu, S.J., Cao, X., Wu, K.L., Cheong, W.C., Chen, Z., Wang, Y., Li, Y., Liu, Y.Q., Wang, D.S., Peng, Q., Chen, C., Li, Y.D., 2018. J. Am. Chem. Soc. 140, 2610–2618.
Peng, B.G., Cui, J.W., Wang, Y., Liu, J.Q., Zheng, H.M., Jin, L., Zhang, X.Y., Zhang, Y., Wu, Y.C., 2018. Nanoscale 10, 1939–1945.
Peng, M., Guan, G.J., Deng, H., Han, B., Tian, C., Zhuang, J.Y., Xu, Y.Y., Liu, W.Z., Lin, Z., 2019. Environ. Sci.: Nano 6, 207–215.
Qin, X.L., Zhang, X.H., Wang, M.H., Dong, Y.F., Liu, J.J., Zhu, Z.W., Li, M.X., Yang, D., Shao, Y.H., 2018. Anal. Chem. 90, 11622–11628.
Qiu, Q.M., Chen, H.Y., Wang, Y.X., Ying, Y.B., 2019. Coord. Chem. Rev. 387, 60–78.
Shao, H.L., Lin, H., Lu, J., Hu, Y.F., Wang, S., Huang, Y.J., Guo, Z.Y., 2018. Biosens. Bioelectron. 118, 247–252.
Shao, K., Wang, B.R., Nie, A.X., Ye, S.Y., Ma, J., Li, Z.H., Lv, Z.C., Han, H.Y., 2018. Biosens. Bioelectron. 118, 160–166.
Shen, H., Liu, J.T., Lei, J.P., Ju, H.X., 2018. Chem. Commun. 54, 9155–9158.
Shu, Y., Yan, Y., Chen, J.Y., Xu, Q., Pang, H., Hu, X.Y., 2017. ACS Appl. Mater. Interfaces 9, 22342–22349.
Tang, Z.Y., He, J.L., Chen, J., Niu, Y.Z., Zhao, Y.L., Zhang, Y.C., Yu, C., 2018. Biosens. Bioelectron. 101, 253–259.
Valizadeh, H., Tashkhourian, J., Abbaspour, A., 2019. Microchim. Acta 186, 455.
Wang, Q.X., Yang, Y.Z., Gao, F., Ni, J.C., Zhang, Y.H., Lin, Z.Y., 2016. ACS Appl. Mater. Interfaces 8, 32477–32487.
Wang, S.S., Zhao, Y.Y., Wang, M.M., Li, H.J., Saqib, M., Ge, C.H., Zhang, X.D., Jin, Y.D., 2019. Anal. Chem. 91, 3048–3054.
Wang, S.Z., McGuirk, C.M., Ross, M.B., Wang, S.Y., Chen, P.C., Xing, H., Liu, Y., Mirkin, C.A., 2017. J. Am. Chem. Soc. 139, 9827–9830.
Wang, X., Yang, C.L., hu, S.J., Yan, M., Ge, S.G., Yu, J.H., 2017. Biosens. Bioelectron. 87, 108–115.
Wang, X.G., Cheng, Q., Yu, Y., Zhang, X.Z., 2018. Angew. Chem. Int. Ed. 57, 7836–7840.
Wang, Y., Wang, L., Chen, H.H., Hu, X.Y., Ma, S.Q., 2016. ACS Appl. Mater. Interfaces 8, 18173–18181.
Wang, Y., Yin, H.S., Li, X.H., Waterhouse, G.I.N., Ai, S.Y., 2019. Biosens. Bioelectron. 131, 163–170.
Wang, Z.H., Yan, Z.Y., Wang, F., Cai, J.B., Guo, L., Su, J.K., Liu, Y., 2017. Biosens. Bioelectron. 97, 107–114.
Wang, Z.L., Jiang, X.Y., Yuan, R., Chai, Y.Q., 2018. Biosens. Bioelectron. 121, 250–256.
Xin, W.L., Jiang, L.F., Zong, L.P., Zeng, H.B., Shu, G.F., Marks, R., Zhang, X.J., Shan, D., 2018. Sens. Actuators B Chem. 273, 566–573.
Xiong, C.Y., Liang, W.B., Zheng, Y.N., Zhuo, Y., Chai, Y.Q., Yuan, R., 2017. Anal. Chem. 89, 3222–3227.
Xu, R.Y., Wang, Y.F., Duan, X.P., Lu, K.D., Micheroni, D., Hu, A.G., Lin, W.B., 2016. J. Am. Chem. Soc. 138, 2158–2161.
Xu, W., Qin, Z., Hao, Y.T., He, Q., Chen, S., Zhang, Z.S., Peng, D., Wen, H.Y., Chen, J., Qiu, J.F., Li, C.R., 2018. Biosens. Bioelectron. 113, 148–156.
Xu, Y., Yin, X.B., He, X.W., Zhang, Y.K., 2015. Biosens. Bioelectron. 68, 197–203.
Xu, Y.X., Li, Q., Xue, H.G., Pang, H., 2018. Coord. Chem. Rev. 376, 292–318.
Xue, Y.Q., Zheng, S.S., Xue, H.G., Pang, H., 2019. J. Mater. Chem. 7, 7301–7327.
Yan, T.T., Zhu, L.Y., Ju, H.X., Lei, J.P., 2018. Anal. Chem. 90, 14493–14499.
Yan, Z.Y., Wang, F., Deng, P.Y., Wang, Y., Cai, K., Chen, Y.H., Wang, Z.H., Liu, Y., 2018. Biosens. Bioelectron. 109, 132–138.
Yang, R.Y., Yan, X.X., Li, Y.M., Zhang, X.H., Chen, J.H., 2017. ACS Appl. Mater. Interfaces 9, 42482–42491.
Yang, X., Lv, J.J., Yang, Z.H., Yuan, R., Chai, Y.Q., 2017. Anal. Chem. 89, 11636–11640.
Yang, Y., Hu, G.B., Liang, W.B., Yao, L.Y., Huang, W., Yuan, R., Xiao, D.R., 2019. Nanoscale 11, 10056–10063.
Yu, Y.J., Yu, C., Niu, Y.Z., Chen, J., Zhao, Y.L., Zhang, Y.C., Gao, R.F., He, J.L., 2018. Biosens. Bioelectron. 101, 297–303.
Zhan, W.W., Kuang, Q., Zhou, J.Z., Kong, X.J., Xie, Z.X., Zheng, L.S., 2013. J. Am. Chem. Soc. 135, 1926–1933.
Zhang, G.Y., Cai, C., Cosnier, S., Zeng, H.B., Zhang, X.J., Shan, D., 2016. Nanoscale 8, 11649–11657.
Zhang, G.Y., Shan, D., Dong, H.F., Cosnier, S., Al-Ghanim, K.A., Ahmad, Z., Mahboob, S., Zhang, X.J., 2018. Anal. Chem. 90, 12284–12291.
Zhang, G.Y., Zhuang, Y.H., Shan, D., Su, G.F., Cosnier, S., Zhang, X.J., 2016. Anal. Chem. 88, 11207–11212.
Zhang, X., Peng, J.J., Song, Y.B., Chen, Y.W., Lu, F.S., Gao, W.H., 2019. Biosens. Bioelectron. 133, 125–132.
Zhang, Y., Wang, F.M., Liu, C.Q., Wang, Z.Z., Kang, L.H., Huang, Y.Y., Dong, K., Ren, J.S., Qu, X.G., 2018. ACS Nano 12, 651–661.
Zhang, Y.X., Xu, J.Y., Xia, J.F., Zhang, F.F., Wang, Z.H., 2018. ACS Appl. Mater. Interfaces 10, 39151–39160.
Zhao, G.H., Wang, Y.G., Li, X.J., Yue, Q., Dong, X., Du, B., Cao, W., Wei, Q., 2019. Anal. Chem. 91, 1989–1996.
Zhao, M.T., Huang, Y., Peng, Y.W., Huang, Z.Q., Ma, Q.L., Zhang, H., 2018. Chem. Soc. Rev. 47, 6267–6295.
Zhao, S.L., Wang, Y., Dong, J.C., He, C.T., Yin, H.J., An, P.F., Zhao, K., Zhang, X.F., Gao, C., Zhang, L.J., Lv, J.W., Wang, J.X., Zhang, J.Q., Khattak, A.M., Khan, N.A., Wei, Z.X., Zhang, J., Liu, S.Q., Zhao, H.J., Tang, Z.Y., 2016. Nat. Energy 1, 16184.
Zhong, M., Yang, L., Yang, H., Cheng, C., Deng, W.F., Tan, Y.M., Xie, Q.J., Yao, S.Z., 2019. Biosens. Bioelectron. 126, 493–500.
Zhou, N., Su, F.F., Guo, C.P., He, L.H., Jia, Z.K., Wang, M.H., Jia, Q.J., Zhang, Z.H., Lu, S. Y., 2019. Biosens. Bioelectron. 123, 51–58.
Zhu, S., Lin, X., Ran, P.Y., Xia, Q., Yang, C.C., Ma, J., Fu, Y.Z., 2017. Biosens. Bioelectron. 91, 436–440.